Online-Journals.org

iJOE International Journal of Online and Biomedical Engineering

iJOE | eISSN: 2626-8493 | Vol. 20 No. 7 (2024) | OPEN ACCESS

https://doi.org/10.3991/ijoe.v20i07.47373

PAPER

Characterization and Identification of Dependence in EMG Signals from Action Potentials and Random Firing Patterns

Gabriela León, Emily López, Hans López, Cesar Hernandez(✉)

Universidad Distrital Francisco José de Caldas, Bogotá D.C., Colombia

cahernandezs@udistrital.edu.co

ABSTRACT

Electromyographic (EMG) signals are biomedical signals that represent neuromuscular activities. The EMG signal is neither stationary nor periodic and exhibits complex interference patterns of several single motor unit action potentials (SMUAPs). This study aims to characterize EMG signals concerning firing patterns and other characteristics and to identify whether these MUAP firing patterns present short-range dependencies (SRD) or long-range dependencies (LRD). To do so, we characterized 208 EMG signals in terms of the number of phases, turns and combinations of phases. Then, we performed a statistical comparison of the (more efficient) Variance-time plot against the (less bias) Log-scale diagram for the estimation of the Hurst parameter and detection of LRD. Using these estimators, we managed to detect LRD in a sample taken with needle electrodes. In contrast, the tools used for the dependence identification on signals achieved with surface electrodes did not yield conclusive results on such dependence.

KEYWORDS

action potential, EMG, LRD, MUAP, SMUAP

1 INTRODUCTION

Physiological processes are complex phenomena, of which nervous or hormonal stimulation and control are part; these are inputs and outputs that can take the form of physical material, neurotransmitters or information, and actions that can be mechanical, electrical, or biochemical. These processes are accompanied by signals that reflect their nature and activities [1].

Throughout time, these signals from the body have been one of the biggest unknowns in the study of the understanding of the human being. These bioelectrical signals fulfill different functions depending on the area of activation for which they are destined. Among the most studied signals are electrocardiographic (ECG),

León, G., López, E., López, H., Hernandez, C. (2024). Characterization and Identification of Dependence in EMG Signals from Action Potentials and Random Firing Patterns. *International Journal of Online and Biomedical Engineering (iJOE)*, 20(7), pp. 48–68. https://doi.org/10.3991/ijoe.v20i07.47373

Article submitted 2023-12-14. Revision uploaded 2024-02-10. Final acceptance 2024-02-11.

photoplethysmographic (PPG), encephalographic (EEG), and electromyographic (EMG) signals, and the last one will be the object of study of this work. EMG signals are biomedical signals that represent contractions that occur in response to a single stimulus, creating a propagated action potential and representing neuromuscular activities [2, 3].

The EMG signal does not have waveforms that can be easily identified; in fact, they are complex interference patterns of innumerable single motor unit action potentials (SMUAPs) [1]. Therefore, an EMG signal does not present a recognizable structure different from an ECG signal. Additionally, these signals are neither stationary nor periodic, and their duration depends directly on the movement performed at the instant of measurement. However, depending on how their measurement is performed, different voltage and frequency ranges can be divided into three types: single fiber electromyography signals (SFEMG), which are normally measured with a needle EMG electrode or a concentric facial needle electrode; the motor unit action potential (MUAP), which represents the changes generated by the motor unit (MU) and is measured with needle electrodes [4]; and finally, surface electromyography signals (EMG), which are obtained with a surface electrode [5].

Although quantitative analysis techniques have been developed to standardize the analysis of the data provided by EMG signals and related to these when obtained with needle electrodes, it is often difficult to extrapolate the structure and activation of the surrounding muscle tissue [6]. So, using simulation or synthetic EMG signal generation, the structure and activation of muscles could be explored. But if this artificial generation of signals is not carried out based on their physiology and without considering the signal's characteristics, including its range dependence, a similar signal to the one produced by the human body would not be obtained, and its study would not be appropriate.

Inter-discharge interval (IDI) characterization of motor unit firing patterns has been studied in very selected works. In [7], the researchers model the distribution of IDI including accommodation for false positives and false negatives, and in [8], they derive an exact solution to the distribution when a gamma distribution is used to model the physiological firing pattern. However, none of them study the presence of long-range dependence (LRD) in the firing patterns of EMG signals.

In this sense, we have set the goal of developing a synthetic EMG signal generator that would allow us to configure the most significant parameters, such as the number of SMUAPs, the number of phases and turns of them, and being able to recreate the firing pattern. In the latter, the identification of short-range dependence (SRD) or long-range dependence of the IDI is of significant importance for two reasons: the first is that although LRD has been detected in other types of biological signals (as in the case of RR intervals of an ECG signal), no evidence has been found, in the literature consulted, that the existence of LRD in the firing patterns of EMG signals has been studied; the second is that, if the LRD is detected in this type of signals, the complexity of the generator would increase significantly, since the generation of random numbers with long range dependence is an area of research that is still in development, which makes part of our research interests, and which contrasts with the random generation of independent numbers (which can be easily solved with the help of the inverse transformation method). For these reasons, we have decided to divide the project into two parts, with the characterization of the EMG signals and the identification of the dependence of the IDI being the objectives to be pursued with this first work.

The characterization of the EMG signals was performed through a literature review, as well as databases of actual signs taken with needle electrodes from the emglab.net website. Using the MATLAB application EMGLAB, some signals were filtered, and all of the cues were decomposed into SMUAP. Once obtained, the characteristics to be reviewed in on the decomposed signals were decided, such as duration, the total

number of data points, their temporal and spatial recruitment, the number of SMUAP, the waveform of each the SMUAP, and percentage of appearance of each SMUAP in the signal. Finally, in this phase, identification and classification were performed for each waveform found according to its turns and stages. The identification of SRD or LRD was carried out through a *Variance-Time Diagram* and a *Log-Scale Diagram*, first with numbers that present independence, then with the bias identification with dependent numbers, and ending with obtaining the Hurst parameter of the SMUAPs.

2 FUNDAMENTALS

2.1 EMG signals

EMG signals are electrical signals produced by a muscle during the contraction and relaxation process; these signals can be used to diagnose pathologies affecting the peripheral nervous system, functional alterations of nerve roots, plexuses, and peripheral nerve trunks, as well as muscle and neuromuscular junction pathologies [9].

Some applications of these signals are the determination of the muscle activation time, the estimation of the force produced by a muscle contraction, and the index of muscle fatigue. The latter applications are highly indicated in sports medicine. Such signals have amplitudes ranging from μV to a low mV range with a frequency range from 50 to 150 Hz [10].

On the other hand, some authors consider that the frequency range of these signals is higher than that of ECG and EEG, ranging from 100 to 10 kHz [11] and of higher amplitude [12]. If this statement is considered, filtering overcomes interference problems that can alter these signals; filtering above 20 Hz can reduce skin potentials and signals from other movements (motion artifacts).

Action Potentials are called motor unit action potential (MUAP). In an electromyographic signal, the most basic concept is called the motor unit (MU), which represents the anatomical and functional elements of the neuromuscular system [13]. The MU is formed by the alpha spinal motor neuron and its corresponding set of innervated cells; the changes generated by the activity of the MU are acquired and amplified using electrodes located in the muscle mass, called motor unit action potential (MUAP) [14]. Each MUAP can be analyzed as a Dirac pulse train, which, when passed through an LTI system, allows the production of the corresponding waveforms, thus allowing it to be implemented in an EMG signal generator.

MUAP Waveforms are characterized by a series of parameters related to aspects of the structure and physiology of the motor unit. So, features such as duration and basic parameters in electromyography define the limits of the MUAP waveform and its period [13].

Figure 1 shows the principal waveforms that can occur in MUAPs. In the context of electromyography, the phases represent the polarity of the waveform. Additionally, several local maxima and minima (referred to as turns) can occur in each stage, as shown in Figure 2.

Firing Patterns are defined by Nikolic [15] as the temporal activation of the motor unit; graphically, they are considered a vertical line on the time axis. Firing patterns give information about the function of the central nervous system and the control of the MUs. Firing trains can be found in different ways; generally, these are found by the excitation and inhibition correlation between movements [16].

Recruitment of MUAPs is the successive activation of the same or different MUs, with increasing force applied at the time of voluntary muscle contraction.

There are two types of recruitment: spatial recruitment, by activating new motor units with increasing effort; and temporal recruitment, by increasing the frequency of discharge (firing rate) of each motor unit with increasing effort [17].

MUs are recruited according to their size. When the muscle is activated, the first MUs to fire are weak and small (lacking in the degree of tension they can generate). But progressively, larger motor units are recruited, which causes an increase in muscle contraction, as seen in Figure 3 [18].

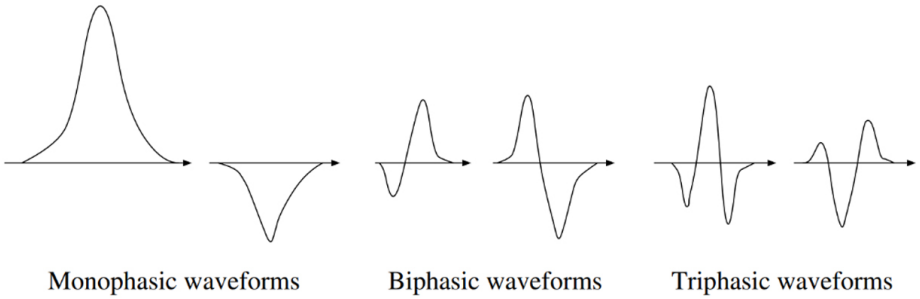

Fig. 1. Representation of single-phase, two-phase, and three-phase waveforms. Adapted from [19]

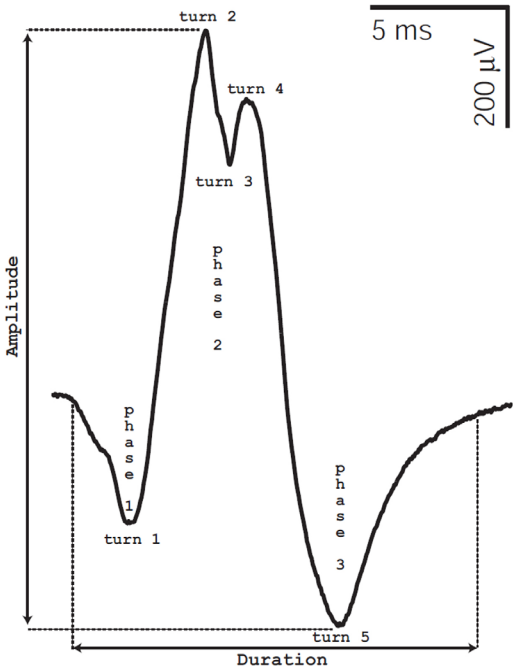

Fig. 2. Illustration of a MUAP waveform. Adapted from [15]

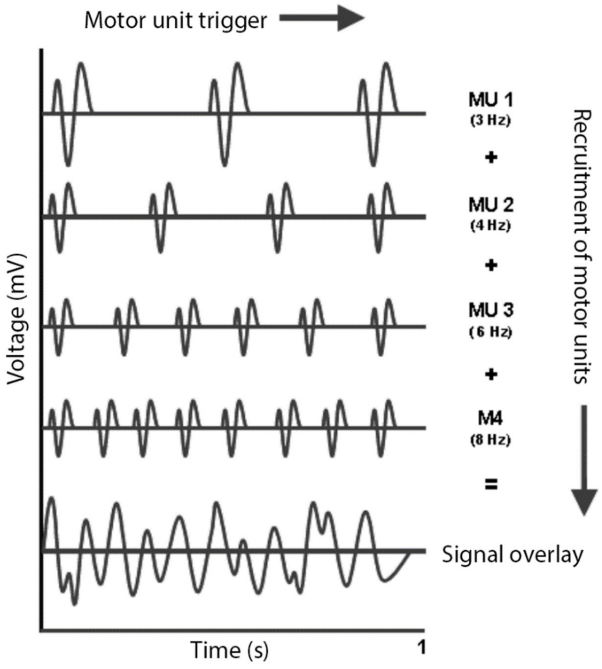

Fig. 3. The recruitment and firing frequency of motor units force output and is reflected in the EMG signal in the superposition. Adapted from [18]

2.2 Short- and long-range dependence

For a discrete-time stochastic process, $X[k]$, $k \in \mathbb{N}$ where $X[k]$ could represent the time sequence between R spikes, the instantaneous periods of a PPG signal, the time between firings of a motor neuron, etcetera. In general, $X[k]$ is a discrete sequence that represents the values of interest, or under study, of a stochastic process a given at time k [20, 21].

Taking into account the role of second-order stationary auto similarity and taking the autocorrelation function $r(k) = \gamma(k) / \sigma^2$, we have equation (1) [22].

$$r(k) \sim H(2H-1)k^{2H-2}, k \to \infty. \quad (1)$$

If $0.5 < H < 1$, $r(k)$ behaves asymptotically as $ck^{-\beta}$ for $0 < \beta < 1$, where $c > 0$ is a constant, $\beta = 2 - 2H$, obtaining equation (2).

$$\sum_{k=-\infty}^{\infty} r(k) = \infty \quad (2)$$

When the autocorrelation function decays slowly, hyperbolically, which is the essential property that causes it to be not summable, as it is shown in equation (2), $X[k]$ is called long-range dependent (LRD). When $H = 0.5$, then $r(k) = 0$ and equation (2) does not hold, so $X[k]$ is called short-range dependent (SRD) by virtue of being completely uncorrelated. The LRD refers directly to the self-similarity between data in its simplest models since, with this model, the dependence can be characterized by a single parameter called the Hurst parameter (H) [23].

Among the simplest methods for estimating the Hurst parameter are the variance-time diagram and the Log scale diagram.

The aggregated process of $X[k]$ is defined, at the aggregation level m, as the discrete sequence $X^{(m)}$, composed by the sample means of consecutive data groups, of size m, as shown in (3). If the process $X[k]$ is exactly or asymptotically self-similar, the logarithm of the sample variance of the aggregate process is (4) [24].

$$X^{(m)}[i] = \frac{1}{m} \sum_{k=m(i-1)+1}^{mi} X[k] \quad (3)$$

$$\log S^2_{X^{(m)}} = \log \sigma^2_X + (2H-2) \log m \quad (4)$$

The **Variance-Time Diagram** is the graph of $\log S^2_{X^{(m)}}$ versus $\log m$, where H can be obtained by estimating the slope $2H - 2$ using linear regression.

Log-Scale Diagram is based on the discrete wavelet decomposition (DWT) of the stochastic process $X[k]$, calculating with them the detail coefficients using a bank of filters with different sampling rates. Since the second moment of the DWT detail coefficients follows a power law with an exponent $2H - 1$, the Hurst parameter can be estimated with equation (5), where μ_j is the arithmetic mean of the squared magnitude of the detail coefficients at octave j and C is a constant. The plot of y_j vs j is known as the (second order) log-scale diagram [22].

$$y_j = log_2 \mu_j = (2H-1)j + log_2 C \quad (5)$$

2.3 EMGLAB

EMGLAB is a MATLAB program for viewing EMG signals, decomposing them into MUAP trains and averaging MUAP waveforms. It provides a convenient graphical interface for displaying and editing results and advanced algorithms for matching templates, resolving overlaps, and averaging by decomposition [15, 24]. The program allows the decomposition of single and multichannel EMG signals into their action potentials.

3 CHARACTERIZATION OF EMG SIGNALS

This section presents the characterization of EMG signals regarding databases, firing patterns, waveforms, and recruitment.

3.1 Databases and decomposition software

The EMG signals used for characterization were taken from the EMGLAB.net website from two databases: clinical signals and real signals [23]. The names of "clinical" and "real" were taken from [23] for referential purposes, and it is necessary to clarify that none of them were synthetic signals; in fact, the signals of both databases were recorded in clinical and laboratory conditions. Both databases were selected because they offer a heterogeneous sample of healthy and not healthy patients, making the characterization more meaningful. In this vein, the material of the first database consisted of a normal control group, a group of patients with myopathy and a group of patients with ALS. The database is composed of EMG signals recorded under normal conditions for analysis by MUAP, produced with a low level of contraction, with a concentric needle electrode; this signal was recorded with 5 points in the muscle and three levels of insertion, deep, medium, and low. High-pass and low-pass filters of 2 Hz and 10 kHz were used, respectively [15]. On the other hand, the second database has eleven sub-databases, according to the method with which the signal was captured and the type of contraction presented.

In addition, and as presented by Nikolic [15] and McGill [24], the software named EMGLAB allows the decomposition of the EMG signals (see Figure 4) provided in their different firing patterns and their waveforms. It should be clarified that the software decomposes correctly within ±0.5 ms at least 98% of the time, and MUAPs presenting peak amplitudes between 1.0 and 2.5 times the amplitude of the RMS signal can be misplaced up to ±5 ms up to 10% of the time [24].

Figure 4 shows an example of a signal decomposition from the clinical signal database. In the upper part, the EMG signal used is in white, and the processed signal is in yellow. In the next window, the number of SMUAPs is shown, as are their waveforms found in the decomposition. Subsequently, the lower left part shows the firing patterns of each SMUAP, while the lower right part shows the amplitude of the desired EMG signal.

Fig. 4. EMGLAB program view

3.2 Trigger patterns

The firing pattern can be identified as the temporal and spatial combination of the different MUAPs presented by the EMG signal. Figure 5 shows an example of a trigger pattern identified by EMGLAB from an actual EMG signal [15].

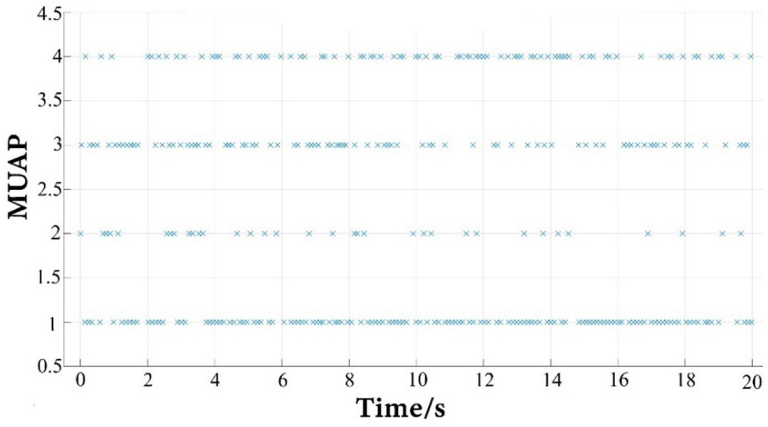

Fig. 5. Firing patterns were identified for the R00503 signal

For this reason, it is relevant to identify the number of individual motor unit action potentials (MUAPs) that can compose an EMG signal, which allows a simple construction process. From these databases, 208 signals were taken to perform their respective feature analysis, and Figure 6 shows the distribution of the number of MUAPs found.

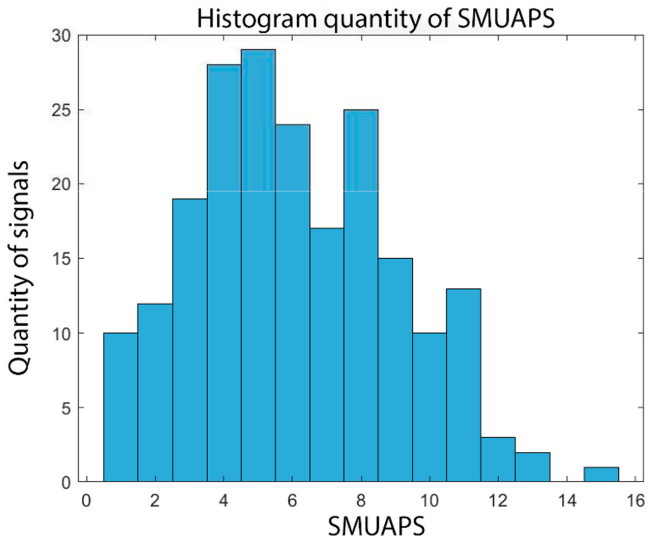

Fig. 6. Distribution of the number of MUAPs for the EMG signals reviewed

In order to simplify some features derived from the identification of the signal firing patterns, a code was implemented in MATLAB to separate the firing pattern of each identified SMUAP from each signal, see Figure 7.

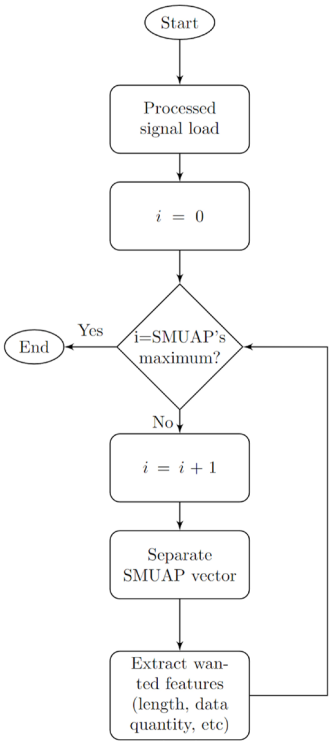

Fig. 7. SMUAP separation code flowchart

3.3 Waveforms

Once the potentials are completely identified, a distinction is made between with the results obtained by the program and the identifying equal waveforms of each firing pattern. Therefore, Figure 8 shows the phase distribution obtained for the 1236 SMUAPs obtained through the EMGLAB software.

On the other hand, each SMUAP presents different phase signs (positive or negative), i.e., two motor units can represent the same number of phases but different signs, indicating that it is a different waveform. Similarly, the number of turns displayed in the signal (number of curves) may vary, which may be equal to or greater than the number of phases of the SMUAPs. The obtained distribution of the number of turns for the 1236 SMUAPs generated by the EMGLAB software is presented in Figure 9.

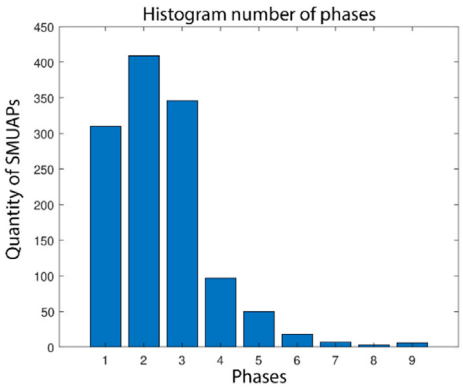

Fig. 8. Distribution of the number of phases for the SMUAPs of the EMG signals reviewed

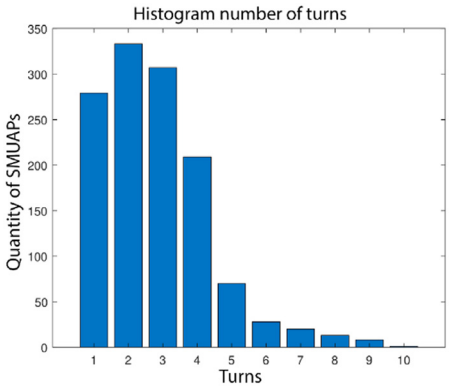

Fig. 9. Distribution of the number of turns for the SMUAPs of the EMG signals reviewed

Figure 10 shows different waveforms representing various examples of the potentials identified by EMGLAB, where diverse numbers of turns are presented. Likewise, Table 1 summarizes the previous characteristics (number of phases, turns, and polarity of phase signs).

Although up to nine phases and ten turns were identified in the SMUAP signals studied, Figure 8 shows that the number of turns is significantly reduced around seven stages. Similarly, Figure 9 shows a significant decrease in the number of turns of the signal between eight and ten. This reduction in the amount is because the noise contained in the sign is comparable to the signal waveform, so it is confused as an additional turn or phase.

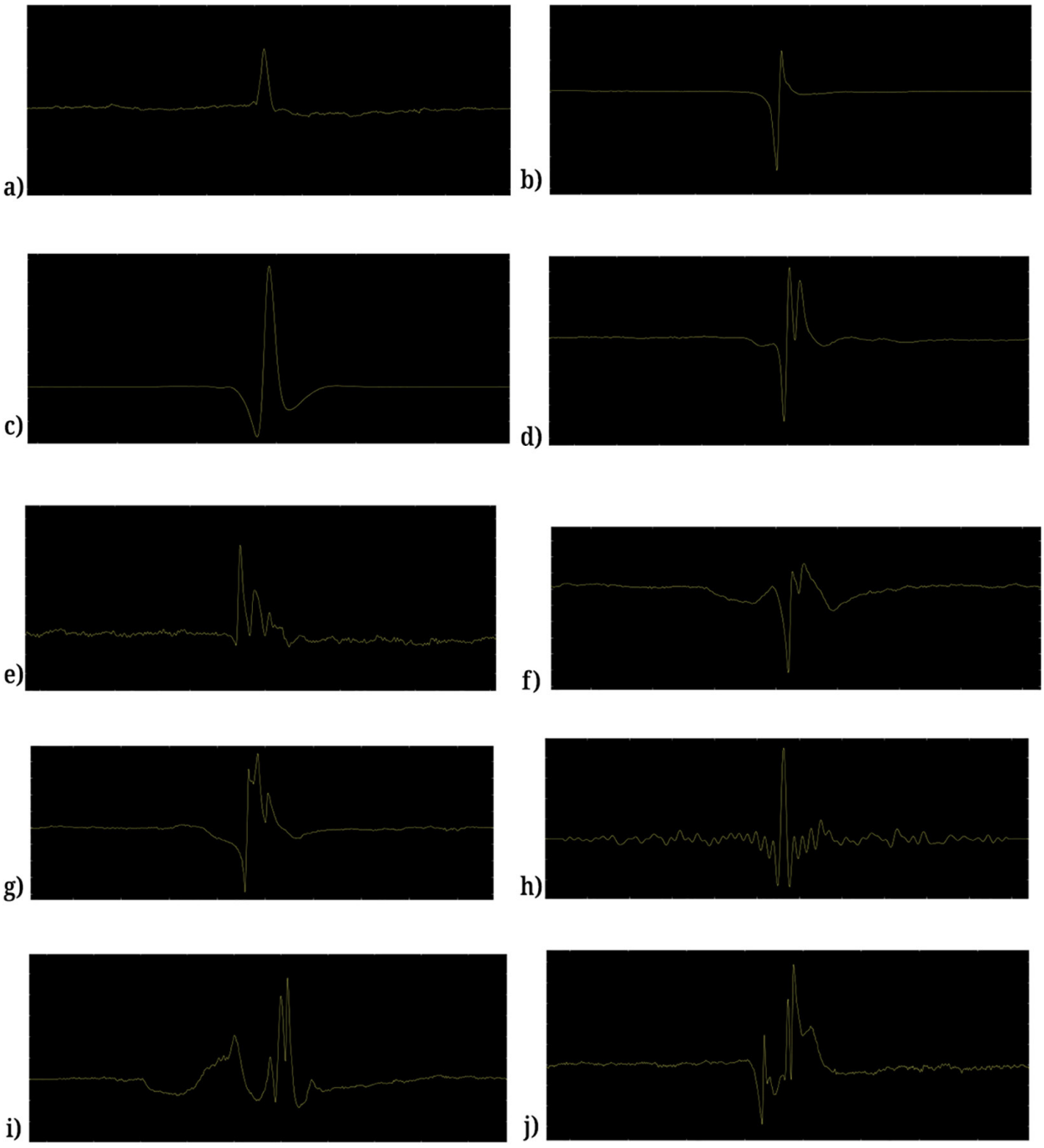

Fig. 10. Examples of the turns of the SMUAPs found

Table 1. Sample of the phase specifications of the SMUAPs were obtained

Phase	Combination	Turns	Amount	Phase	Combination	Turns	Amount
1	+	1	238	5	−+−+−	5	12
	−	1	41		+−+−+	5	28
	++	2	7		+−++−+	6	2
	−−	2	1		−+−++−	6	2
	+++	3	35		+−−+−+	6	1
	−−−	3	3		−−−+−−−+−	9	1
	++++	4	2		+−+−+++	7	1
	−−−−	4	1		+−++−+	7	3
	+++++	5	2		++−−−+−−++	10	1
2	−+	2	266	7	−+−+−+−	7	4
	+−	2	59		+−+−+−+	7	2
	−++	3	19		+−+−+++−+	9	1
	−−+	3	7	8	+−+−+−+	8	3
	−+++	4	48	9	+−+−+−+−+	9	2
	−−−+	4	3		−+−+−+−+−	9	4
	−−++	4	5				
	−−−+++	6	2				

3.4 Recruitment

Recruitment is divided into two types: temporal and spatial. For the temporal recruitment, a code was created in MATLAB software (see Figure 7), in which the decomposed signal obtained by EMGLAB is entered to be separated into the MUAPs that were identified. The code generates a two-column array where the time of appearance and the number of the identified MUAP are found, with the first column being the intermediate appearance times.

For spatial recruitment, it is indispensable to consider the beginning and end of each identified SMUAP. In addition, considering the total amount of signal data and the amount corresponding to each SMUAP, it is possible to determine the SMUAP percentage of occurrence in each one.

4 DEPENDENCE IDENTIFICATION

There are several tools for dependence estimation, either long-range or short-range. These have been developed over time, and there are several algorithms implemented in software such as MATLAB, that show the Hurst parameter estimation and a graph where the confidence interval on the input sample is identified.

To have accurate statistics on the estimation tools, the behavior of two means for such identification was evaluated, allowing us to estimate the bias they present at the level of precision or accuracy and thus consider the errors in the estimation of the dependence of the electromyographic signals. The selected tools are the *variance-time diagram* and the *log-scale diagram*, for which their behavior was evaluated when reliance between the data was present and not present.

In the search performed and characterization of the EMG signals, it was not possible to find EMG signals of long duration; therefore, it was decided to evaluate the Hurst parameter estimation tools with the average duration value of the signals found for the characterization, with a considerable minimum of 800 data points, understanding that the error is reduced for longer sequences.

For the development of these tests on the estimators, it was decided to divide them into two parts: random numbers without dependence and random numbers with dependence. In the first, the Hurst parameter is 0.5, and these random numbers generated in the MATLAB software have a normal distribution. Figure 11a shows the flow chart summarizing the algorithm used.

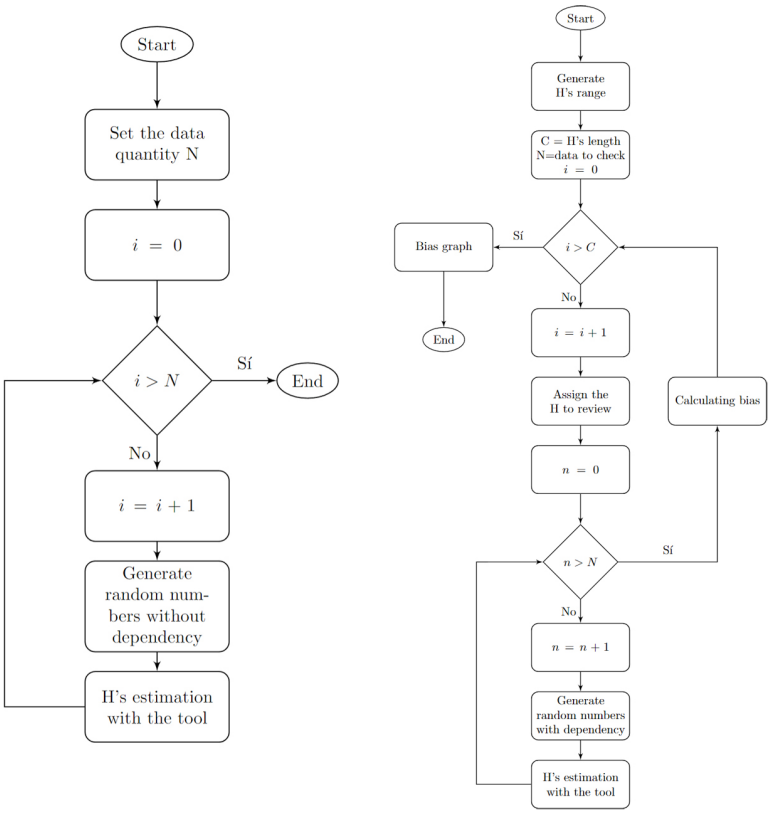

Fig. 11. Flowchart of the bias checking algorithm of the tools (a) for numbers with no dependence and (b) for numbers that have a specific dependence

On the other hand, the second test of the tool must be performed with numbers with dependence generated with the Multifractal Wavelet Model (MWM). In the MWM, a symmetric beta distribution is used in a multiplicative cascade where the desired Hurst parameter can be indicated. Figure 11b shows the flow chart summarizing the algorithm used for this test.

Equation (6) was used to determine the bias in the tests.

$$\text{Bias} = \hat{\text{E}}(H) - H_{Theoretical} \tag{6}$$

4.1 Variance-time diagram

The Hurst exponent has been widely used in different fields as a measure of long-range dependence in time series. The variance-time plot analysis is based on the

slowly decomposing variance property of self-similar processes undergoing aggregation [25]. In [26], it is stated that it is based on the asymptotic relationship of the variance of sample averages. In the case of having a small amount of statistical data for the observation, the plot only allows for verifying if the time series is self-similar. If it is, it grants obtaining the approximate estimate of the Hurst parameter. For this reason, the tool has several shortcomings because it requires large sample sizes and an arbitrary level of aggregation [27].

Tests of the estimation with numbers without dependence. Consists of entering numbers with no dependence between them. This test determines the bias present in this type of data, using an algorithm in MATLAB software to obtain the Hurst parameter. Two different sets of data were used for the Hurst parameter evaluation, the minimum amount of 800 data points and the approximate average amount of 1000 data. It used a normal distribution to check the bias presented by the tool with independent random numbers or SDR, which has a Hurst parameter of 0.5.

Figures 12 and 13 show the distribution presented by the tests with the two amounts of data, where it can be seen that it tends to remain at 0.5.

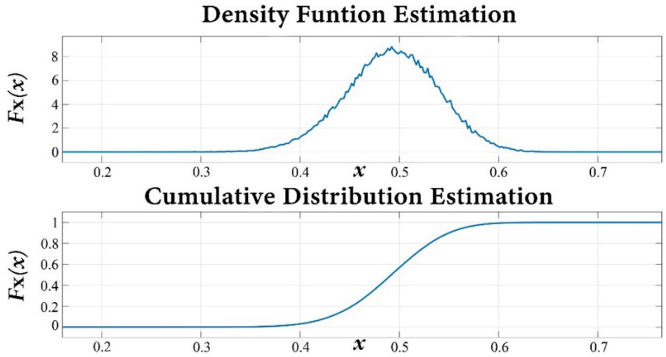

Fig. 12. Density function and cumulative dispersion of the independent data estimation with the vt function with N = 800

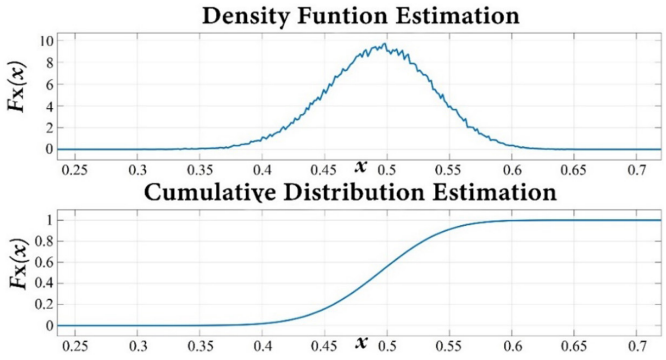

Fig. 13. Density function and cumulative dispersion estimation of the independent data with the vt function with N = 1000

Finally, Table 2 shows the biases obtained in the algorithm application to obtain the variance-time diagram with data that does do not show dependence. As can be seen, the range of error presented by the algorithm is considerable, but it is maintained at a low value.

Table 2. The bias of the variance-time tool with numbers without dependence

No. Data	Maximum Bias
800	–0.0072
1000	–0.0059

Tests of the estimation with numbers with dependence. In the study of estimators, [27] stated that the variance-time estimation tool, when LRD is present in the study sample, presents a representative bias when the self-similarity of the data increases. As a demonstration, a MATLAB algorithm was used to determine the bias about the Hurst parameter presented, which is summarized in Figure 11b.

Figures 14 and 15 show the relationship of the bias with the Hurst parameter with two different numbers of iterations. As mentioned above, it depends on the amount of data that have the signals to be used for identification, and the tool that generates the random numbers handles data lengths in base 2, with a data length of 1024.

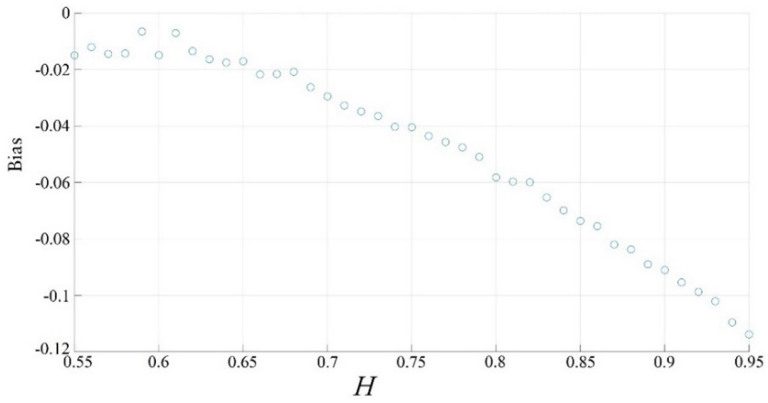

Fig. 14. Relationship of bias with Hurst parameter for N = 800

Finally, Table 3 shows the highest value biases obtained in the algorithm application to obtain the variance-time diagram with data that present dependence between them. As can be seen, the error range presented by the algorithm with data that have reliance between them increases concerning those without dependence. So, dependence could be detected for estimates greater than 0.6139 in discrete sequences of 1024 samples.

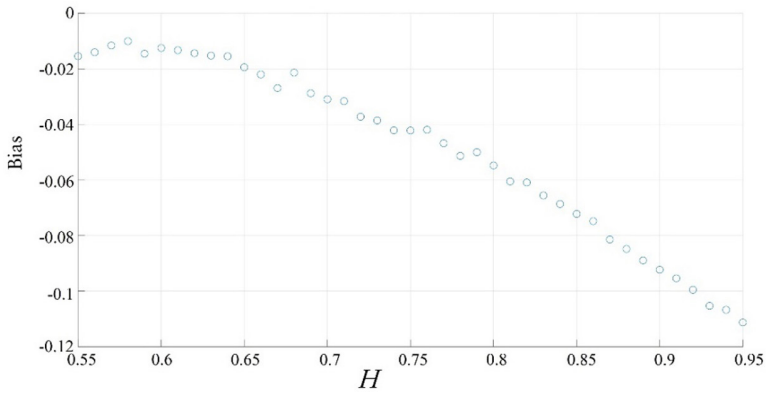

Fig. 15. Relationship of the bias with the Hurst parameter for N = 1000

Table 3. The bias of the variance-time tool with numbers with dependence

Iterations	Average Bias	Maximum Bias
800	–0.0480	–0.1139
1000	–0.0486	–0.1113

4.2 Log-scale diagram

Several methods have been developed that allow the calculation of the Hurst exponent from experimental data; among them is the calculation with the detail coefficients of the Discrete Wavelet Transform. This method has shown that estimates with Wavelets are highly unbiased and stable in the presence of deterministic trends [27].

Tests of the estimation with numbers without Dependence. Firstly, and as in the procedure performed for the variance-time diagram, the study of the tool is carried out when the data entered into it do not depend on each other, being random. The algorithm described in the diagram in Figure 11a is used in MATLAB software with which the Hurst parameter is obtained. Similarly, the highest concentration of data produced randomly by MATLAB is expected to be around 0.5.

Figures 16 and 17 show the distribution presented by the tests with the two amounts of data. In these, it tends to concentrate around 0.5.

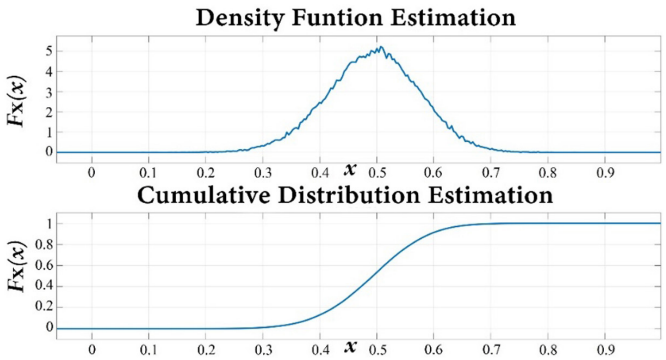

Fig. 16. Estimation of the cumulative density and dispersion function of the independent data with the LD function with N = 800

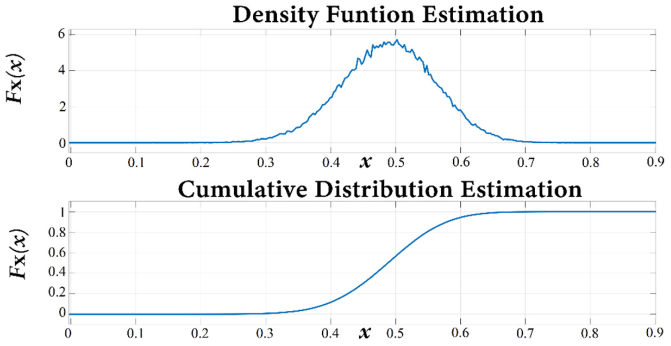

Fig. 17. Estimation of the cumulative density and dispersion function of the independent data with the LD function with N = 1000

Finally, Table 4 shows the biases obtained in the algorithm application to obtain the log-scale diagram with data without dependence. As can be seen, the error range presented by the algorithm with data without dependence is smaller than the one raised with the variance-time diagram for a smaller amount of data, but it is larger when there is more data.

Table 4. The bias of the log-scale tool with numbers without dependence

No. Data	Maximum Bias
800	–0.0052
1000	–0.0103

Testing the estimation with numbers with dependence. Wavelets are an excellent mathematical tool that allow the analysis of signals and images in several dimensions. The Discrete Wavelet Transform (DWT) can reconstruct time series perfectly, so it is a suitable method for processes that present LRD [28, 29].

Figures 18 and 19 show the bias relationship with the Hurst parameter with the two amounts of iterations established. As mentioned above, it depends on the amount of data that signals have to be used for identification, and the tool that generates the random numbers handles data lengths with base 2, with a length of 1024.

As observed in Figures 18 and 19, the bias does not present a clear trend, oscillating highly and causing inconclusive results. This is due to the small number of iterations used for the estimation, so it was decided to perform a new test with a large number of iterations (N = 100000), obtaining the results presented in Figure 20.

As seen in Figure 20, by having a higher amount of data for the Hurst parameter calculation, the bias tends to decrease in amplitude, decreasing the error presented when using the algorithm.

Finally, Table 5 shows the biases obtained in the algorithm application to obtain the log-scale diagram with data that show dependence between them. It presents a lower bias than the one obtained in the experimentation with the variance-time diagram.

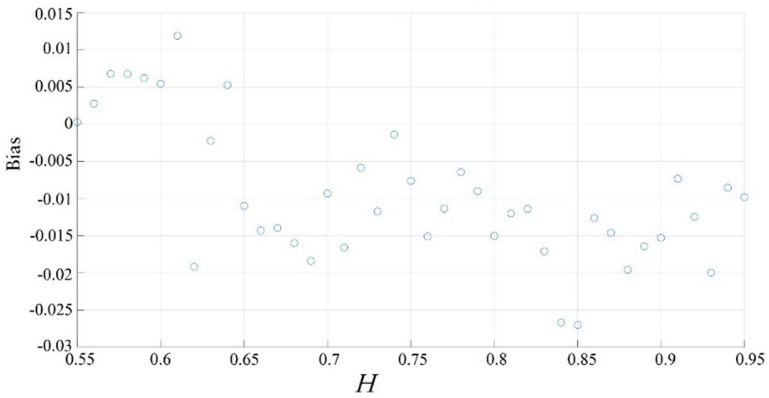

Fig. 18. Relationship of bias to Hurst parameter for N = 800

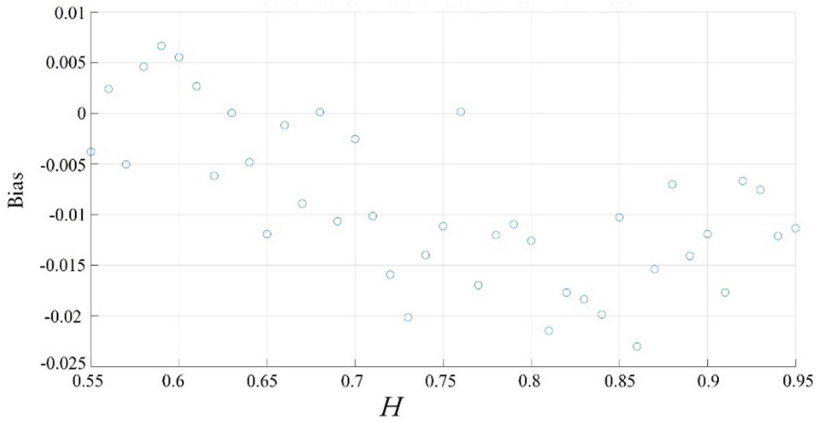

Fig. 19. Relationship of the bias with the Hurst parameter for N = 1000

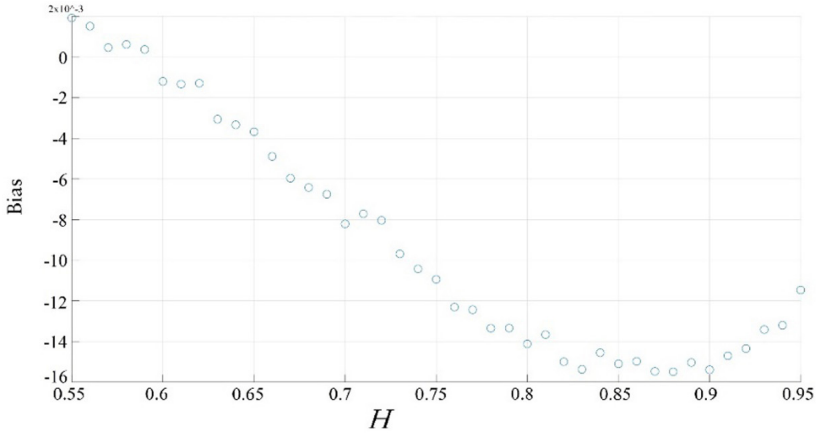

Fig. 20. Relationship of the bias with the Hurst parameter for N = 100000

Table 5. The bias of the log-scale tool with numbers without dependence

Iterations	Average Bias	Maximum Bias
800	–0.0095	±0.0270
1000	–0.0090	±0.0230
100000	–0.0090	±0.0155

4.3 Signals used for the identification of dependence and their results

To identify the type of dependence presented by the electromyographic signals, a sample of those used for the characterization was selected. The selection of this sample was based mainly on the amount of data in the sign depending directly on the duration of the signal and taking a minimum total of 800 data points. Table 6 details the signals that meet this condition to obtain a fairer dependence.

Table 6. Description of the signals used for the identification of the type of dependence

Signal	Data Quantity	Electrode Type
R00401dc1	1495	Needle
R00401dc2	1484	Needle
R00401dc3	1484	Needle
R00609	801	Needle
R01101C1F500	2584	Superficial
R01102aC1F500	1881	Superficial
R01102bC2F500	999	Superficial

Figure 21 shows the algorithm used to estimate the actual signals with Hurst parameter. The signals shown in Table 6 are the signals to be considered due to their amount of data. Consequently, Table 7 shows the results of the Hurst parameter for those obtained and those corrected with the corresponding bias of the tool, assuming the worst case. This adjustment is calculated using equation (7)

$$\text{Adjustment} = H - \text{Bias} \tag{7}$$

When detailing the results obtained, it is evident that the first four signals, when evaluated with the two tools, are above 0.5, and when applying the tool bias, it is noticed that the estimation value increases. This behavior indicates that the signals taken with needle electrodes selected for identification, although they have little data quantity, present long-range dependence between them.

Nevertheless, when the last three signals are evaluated with the two tools, different results are obtained for the R01102aC1F500 signal about the dependence. I.e., with the variance-time tool, the sign has a long-range dependence (it remains above 0.5), while with the log-scale tool, we obtain a short-range dependence indicating an independence between its data (it remains below 0.5). By obtaining different dependencies, we conclude that the results for the signals generated by surface electrodes are not conclusive.

Table 7. Results of the dependence tests on the signals

Signal	VT		LD	
	Estimation	Adjustment with Average Bias	Estimation	Adjustment with Average Bias
R00401dc1	0.6786	0.7266	0.8095	0.8185
R00401dc2	0.7079	0.7559	0.8031	0.8121
R00401dc3	0.7079	0.7559	0.8031	0.8121
R00609	0.6271	0.6751	0.7064	0.7154
R01101C1F500	0.5636	0.6116	0.4973	0.5063
R01102aC1F500	0.5652	0.6132	0.3912	0.4002
R01102bC2F500	0.6137	0.6617	0.5590	0.5680

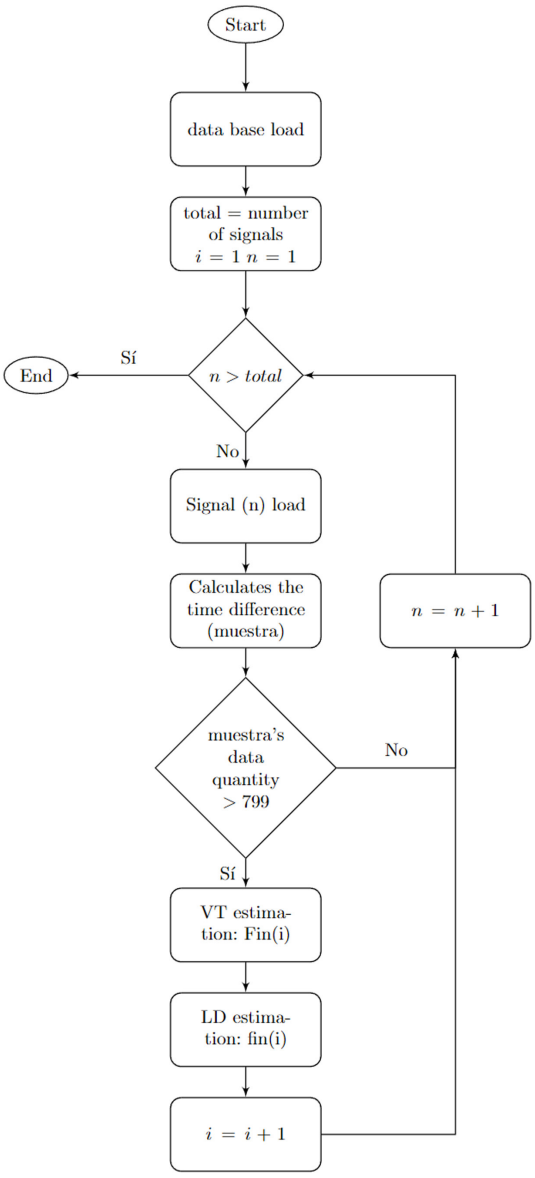

Fig. 21. Flowchart of the algorithm for determining the dependence on real signals

5 CONCLUSIONS

Electromyographic signals have characteristics such as firing trains, spatial recruitment, temporal recruitment, number of turns, and waveform phases, which make their characterization and reconstruction possible. The evidence presented above demonstrates that it is possible to model the generation of electromyographic signals using different statistical (variance-time and log-scale diagrams) and modeling tools.

Even though most of the signals presented less than a thousand data points when performing the dependence tests on the EMG signals that were acquired by needle electrodes from the selected database, a long-range dependence was obtained. In contrast, the tools used for the dependence identification (variance-time and log-scale diagrams) on signals achieved with surface electrodes did not yield

conclusive results on such dependence; this may be because they do not present the same treatment, and the dependence result may vary if adequate signal preprocessing is performed.

Similarly, it is relevant to highlight the results of the estimation tools reviewed. If greater efficiency (precision) is required, the tool to use would be the variance-time diagram since it has a narrower distribution but requires more processing time. On the other hand, if a lower bias (accuracy) is required in the results, the appropriate tool is the Log-scale diagram since it is centered around 0.5; however, it requires a large amount of data to generate adequate results.

According to the results obtained, it is important to highlight that evidence has been found that there is long-range dependence in the firing patterns of EMG signals, which is something new. In order to better support this finding, the capture of EMG signals, with needle electrodes, for a greater amount of time, is proposed as future work. The latter have longer discrete sequences and thus reduce the error in the estimation of the Hurst parameter. The capture of EMG signals for extended periods of time is not usually done, because it is not necessary to apply other algorithms – such as RMS, which allows us to extract an indirect signal from the applied force – so there are no databases that can help us make the task easier.

6 ACKNOWLEDGMENT

The authors thank the Center for Research and Scientific Development of Universidad Distrital Francisco Jose de Caldas for supporting this investigative project.

This research did not receive any specific grant from funding agencies in the public, commercial, or not-for-profit sectors.

7 REFERENCES

[1] R. M. Rangayyan, *Biomedical Signal Analysis a Case-Study Approach*, wiley, 2002. https://doi.org/10.1109/9780470544204

[2] S. Anowarul Fattah, "Identifying the motor neuron disease in EMG signal using time and frequency domain features with comparison," *Signal & Image Processing: An International Journal*, vol. 3, no. 2, 2012. [Online serial]. Available: https://doi.org/10.5121/sipij.2012.3207. [Accessed: Dec. 6, 2023].

[3] C. J. De Luca, "Physiology and mathematics of myoelectric signals," *IEEE Transactions on Biomedical Engineering*, vol. 26, no. 6, 1979. [Online serial]. Available: https://doi.org/10.1109/TBME.1979.326534. [Accessed: Dec. 6, 2023].

[4] A. Selvan, "Single-fiber EMG: A review," *Annals of Indian Academy of Neurology*, para. [2011]. [Online]. Available: https://www.ncbi.nlm.nih.gov/pmc/articles/PMC3108086/.

[5] J. Wu, X. Li, W. Liu, and J. Wang, "sEMG signal processing methods: A review," *Journal of Physics: Conference Series*, vol. 1237, no. 3, 2019. [Online serial]. https://doi.org/10.1088/1742-6596/1237/3/032008

[6] A. Hamilton-Wright and D. Stashuk, "Physiologically based simulation of clinical EMG signals," *IEEE Transactions on Biomedical Engineering*, vol. 52, no. 2, 2005. [Online serial]. Available: https://doi.org/10.1109/TBME.2004.840501. [Accessed: Dec. 6, 2023].

[7] Javier Navallas, Javier Rodriguez-Falces, and Armando Malanda, "Inter-discharge interval distribution of motor unit firing patterns with detection errors," *Transactions on Neural Systems and Rehabilitation Engineering*, vol. 23, no. 2, 2015. https://doi.org/10.1109/TNSRE.2014.2363133. [Accessed: March, 2015].

[8] Javier Navallas, Sonia Porta, and Armando Malanda, "Exact inter-discharge interval distribution of motor unit firing patterns with gamma mode," *Medical & Biological Engineering & Computing*, Available: https://doi.org/10.1007/s11517-018-01947-y. [Accessed: Dec. 20, 2018].

[9] Dalcame, "Electromiografía," *Dalcame*, 2005. [Online]. Available: http://www.dalcame.com/emg.html#.X4o6m9BKjIV. [Accessed: Oct. 16, 2020].

[10] R. Ruiz Rubio, "Aplicaciones de las señales electromiográficas," *Dialnet.com*, para.53, 1999. [Online]. Available: https://www.uma.es/estudios/centros/Ciencias/publicaciones/encuentros/ENCUENTROS53/aplicaciones.html. [Accessed: Oct. 16, 2020].

[11] C. Tabernig, R. Acevedo, and J. Fernández, "Influencia de la fatiga muscular en la señal electromiográfica de músculos estimulados eléctricamente," *Revista EIA*, vol. 2, no. 7, 2007. [Online serial]. Available: https://www.redalyc.org/pdf/1492/149216939009.pdf. [Accessed: Oct.16, 2020].

[12] L. Alvarés, "Acondicionamiento de señales bioeléctricas," *studocu*, para.3, April, 2007. [Online serial]. Available: https://www.studocu.com/es-ar/document/instituto-universitario-del-hospital-italiano/fisiologia/senales-bioelectricas/33951179. [Accessed: Oct. 16, 2020].

[13] I. Rodríguez and L. Gila-Useros, Eds., *Motor Unit Action Potential Duration: Measurement and Significance*. IntechOpen, 2012.

[14] E. Stålberg, S. Nandedkar, D. Sanders, and B. Falck, "Quantitative motor unit potential analysis," *Journal of Clinical Neurophysiology*, vol. 13, no. 5, pp. 401–422, 1996. [Abstract]. Available: ProQuest, https://journals.lww.com/clinicalneurophys/abstract/1996/09000/quantitative_motor_unit_potential_analysis.4.aspx#ContentAccessOptions. [Accessed: Oct. 16, 2020].

[15] M. Nikolic, "Detailed analysis of clinical electromyography signals EMG decomposition, findings and firing pattern analysis in controls and patients with myopathy and amy-trophic lateral sclerosis," in *Faculty of Health Science, University of Copenhagen* Press, 2001. [Online document]. Available: http://www.emglab.net/emglab/Publications/Documents/Miki_Nikolic_PhD_Thesis.pdf. [Accessed: Oct. 16, 2020].

[16] E. Micheli-Tzanakou, *The Biomedical Engineering Handbook. Medical Devices and Systems*. CRC Taylor & Francis, 2006.

[17] P. F. Bereslaswski, "Manejo de los factores nerviosos durante la rehabilitación muscular y aplicación de altas tensiones para la producción de la fuerza," Asociacion de Kinesiología y deportes, para, vol. 3, 2015. [Online]. Available: [Accessed: Oct. 16, 2020].

[18] H. I. Hoyos Daza, "Patrones de actividad muscular en miembros inferiores durante la marcha humana bajo condiciones de alivio de carga corporal," *Pontificia Universidad Javeriana, para*, vol. 3, 2014. [Online]. Available: https://repository.javeriana.edu.co/bitstream/handle/10554/16506/HoyosDazaHectorIvan2014.pdf;sequence=1. [Accessed: Oct. 16, 2020].

[19] R. M. Rangayyan, *Biomedical Signal Analysis*. John Wiley & Sons, 2015. https://doi.org/10.1002/9781119068129

[20] H. I. López-Chávez, "Detección de la LRD en el ritmo cardiaco," Apuntes de clase, 2023.

[21] A. K. Mahabalagiri, K. Ahmed, and F. Schlereth, "A novel approach for simulation, measurement and representation of surface EMG (sEMG) signals," in *Conference Record – Asilomar Conference on Signals, Systems and Computers*, 2011, pp. 476–480. https://doi.org/10.1109/ACSSC.2011.6190045

[22] M. Téllez, J. Mejía, H. López, and C. Hernández, "Random number generator with longrange dependence and multifractal behavior based on Memristor," *Electronics*, vol. 10, no. 9, 2020. [Online serial]. Available: https://doi.org/10.3390/electronics9101607. [Accessed: Oct. 16, 2020].

[23] K. Park and W. Willinger, *Self-Similar Network Traffic and Performance Evaluation*. Barcelona: John Wiley & Sons, 2000. https://doi.org/10.1002/047120644X

[24] S. L. Orozco, G. Cerda, G. A. Cervantes, D. H. Fusilier, and M. T. Cisneros, "Analysis of LRD series with time-varying Hurst parameter," *Computacion y Sistemas*, vol. 13, no. 3, pp. 295–312, 2009. [Abstract]. Available: https://www.redalyc.org/pdf/615/Resumenes/Resumen_61519182005_1.pdf. [Accessed: Oct. 16, 2020].

[25] K. C. McGill, Z. C. Lateva, and H. R. Marateb, "EMGLAB: An interactive EMG decomposition program," *Journal of Neuroscience Methods*, vol. 149, no. 2, pp. 121–133, 2005. [Abstract]. Available: ProQuest, https://doi.org/10.1016/j.jneumeth.2005.05.015. [Accessed: Oct. 16, 2020].

[26] R. F. Ceballos and F. F. Largo, "On the estimation of the Hurst exponent using adjusted rescaled range analysis, detrended fluctuation analysis and variance time plot: A case of exponential distribution," *Imperial Journal of Interdisciplinary Research,* vol. 3, no. 8, pp. 424–434, 2018. [Abstract]. Available: ProQuest, https://arxiv.org/abs/1805.08931. [Accessed: Oct. 16, 2020].

[27] G. Pujolle, H. Perros, S. Fdida, U. Korner, and I. Stavrakakis, "Networking 2000 broadband communications, high performance networking, and performance of communication networks: IFIP-TC6," *European Commission International Conference Paris*, France, vol. 1815, ISBN: 978-3-540-67506-8, 2000. [Online serial]. Available: https://doi.org/10.1007/3-540-45551-5. [Accessed: Oct. 16, 2020].

[28] O. Sheluhin, S. Smolskiy, and A. Osin, *Self-Similar Processes in Telecommunications*. Barcelona: John Wiley & Sons, 2007. https://doi.org/10.1002/9780470062098

[29] R. D. Brooks, E. A. Maharaj, and B. Pellegrini, "Estimation and analysis of the Hurst exponent for Australian stocks using wavelet analysis," *Applied Financial Economics Letters*, vol. 4, no. 1, pp. 41–44, 2008. [Online serial]. Available: https://doi.org/10.1080/17446540701367444. [Accessed: Oct. 16, 2020].

8 AUTHORS

Gabriela León was born in Bogotá, Colombia. She received her bachelor's degrees in electronic engineering from Universidad Distrital Francisco José de Caldas, Colombia. Her research interests include bioengineering and intelligent systems.

Emily López was born in Bogotá, Colombia. She received her bachelor's degrees in electronic engineering from Universidad Distrital Francisco José de Caldas, Colombia. Her research interests include bioengineering and intelligent systems.

Hans López was born in Barranquilla, Colombia. He is master's graduate in information and communications sciences from Universidad Distrital Francisco José de Caldas, Colombia. He is currently a Titular Professor of electronic engineering at Universidad Distrital Francisco José de Caldas. His research interests include statistical signal processing and biological signal processing.

Cesar Hernandez was born in Villavicencio, Colombia. He received bachelor's and master's degrees in electronic engineering and telecommunications from Universidad Distrital Francisco José de Caldas, Colombia, and the Ph.D. degree in engineering from Universidad Nacional de Colombia. He is currently a Titular Professor of electrical engineering programs with Universidad Distrital Francisco José de Caldas. His research interests include mathematical optimization, cognitive radio networks, and intelligent systems (E-mail: cahernandezs@udistrital.edu.co).